Journal of Hazardous Materials 203–204 (2012) 317–325

Contents lists available at SciVerse ScienceDirect

Journal of Hazardous Materials

journal homepage: www.elsevier.com/locate/jhazmat

Role of uniform pore structure and high positive charges in the arsenate adsorption performance of Al_{13}-modified montmorillonite

Shou Zhao [a], Chenghong Feng [a,*], Xiangning Huang [b], Baohua Li [a], Junfeng Niu [a], Zhenyao Shen [a]

[a] Key Laboratory for Water and Sediment Science of Ministry of Education, School of Environment, Beijing Normal University, Beijing 100875, China
[b] School of Civil Engineering, Purdue University, West Lafayette, IN 47907, USA

ARTICLE INFO

Article history:
Received 31 August 2011
Received in revised form 5 December 2011
Accepted 10 December 2011
Available online 19 December 2011

Keywords:
Al_{13}
Modified montmorillonite
Uniform pore structure
Arsenate adsorption
High charge

ABSTRACT

Four modified montmorillonite adsorbents with varied Al_{13} contents (i.e., Na-Mont, AC-Mont, PAC_{20}-Mont, and Al_{13}-Mont) were synthesized and characterized by N_2 adsorption/desorption, X-ray diffraction, and Fourier-transform infrared analyses. The arsenate adsorption performance of the four adsorbents were also investigated to determine the role of intercalated Al_{13}, especially its high purity, high positive charge (+7), and special Keggin structure. With increased Al_{13} content, the physicochemical properties (e.g., surface area, structural uniformity, basal spacing, and pore volume) and adsorption performance of the modified montmorillonites were significantly but disproportionately improved. The adsorption data well fitted the Freundlich and Redlich–Peterson isotherm model, whereas the kinetic data better correlated with the pseudo-second-order kinetic model. The arsenate sorption mechanism of the montmorillonites changed from physical to chemisorption after intercalation with Al_{13}. Increasing charges of the intercalated ions enhanced the arsenate adsorption kinetics, but had minimal effect on the structural changes of the montmorillonites. The uniform pore structure formed by intercalation with high-purity Al_{13} greatly enhanced the pore diffusion and adsorption rate of arsenate, resulting in the high adsorption performance of Al_{13}-Mont.

1. Introduction

Arsenic, being ubiquitous in environment and toxic to humans, presents potentially serious water environmental problems in many countries around the world. To date, as many as 60–100 million people worldwide are at risk of exposure to excessive levels of arsenic. Consequently, stricter regulations on arsenic discharge have been enforced in many countries, also suggested by the World Health Organization. Hence, highly efficient technologies for the removal of this pollutant urgently need to be developed [1].

There are various arsenic removal methods such as precipitation, coagulation, iron-exchange, adsorption, and reverse osmosis. Adsorption is considered as one of the most promising technologies because it is easily executable, highly efficient, and cost effective [2,3]. Adsorbents are generally considered to play dominant roles in adsorption processes. Naturally occurring and modified montmorillonites are widely used in arsenic removal from water and wastewater. These abundant and low-cost adsorbents have high specific surface areas, chemical and mechanical stabilities, and high cation exchange capacities [4]. The surface and structural properties of modified montmorillonites can often be remarkably improved compared with the original materials. The affinity of arsenic for montmorillonite can also be significantly increased after pillaring with cations, especially some polycations [5–8].

Among such polycations, Al_{13} with Keggin structure has gained the most popularity because of its special structure, high molecular weight, and high positive charge. However, most previous studies have only focused on the contributions of the former two Al_{13} characteristics to enhance the surface area, pore volume, and some other physicochemical characters of montmorillonite. In fact, the high positive charge (+7) carried by Al_{13}, which is significantly higher than mono Al species and some other known Al species, may also play an important role in the improvement of the montmorillonite adsorption performance.

In natural waters, arsenic predominantly occurs in such inorganic forms as arsenate and arsenite, referred to as As(V) and As(III), respectively [9,10]. These two forms both carry negative charges in most cases. Montmorillonites also carry negative net charges, which certainly decreases the adsorption strength of arsenic. After modification with Al_{13}, the pillared and adsorbed polycations with high positive charges (+7) may balance the charges of the montmorillonites. As a result, the electrostatic adsorption strength is markedly improved. To our knowledge, little attention has been

* Corresponding author. Tel.: +86 10 5880 4573; fax: +86 10 5880 4573.
E-mail addresses: fengchenghong@hotmail.com, fengchenghong@163.com (C. Feng).

0304-3894/$ – see front matter © 2011 Elsevier B.V. All rights reserved.
doi:10.1016/j.jhazmat.2011.12.035

paid to the effect of charge difference of modifier on the adsorption performance of modified montmorillonite.

Previous studies have reported improved structures and adsorption performances of Al_{13}-modified montmorillonites using simple polymeric Al solutions with a relatively high Al_{13} content [5,11,12]. However, there is almost no report on the role of high Al_{13} purity in the arsenic adsorption performance of modified montmorillonites. Shin and Han [13] have studied phosphate adsorption on aluminum-impregnated mesoporous silicates. They have proven that the uniform mesopores of these silicates cause the diffusion rate to increase significantly, thereby enabling faster adsorption. Hence, the modification of montmorillonites with purified Keggin-Al_{13} might also enhance pore uniformity as well the rate of transfer and adsorption of arsenate.

In the present study, a highly purified Al_{13} solution was synthesized and used to modify montmorillonites. Special attention had been paid to the characteristics of Al_{13} (i.e., high purity, high positive charges, and Keggin structure) in the improvement of arsenic adsorption performance on the modified montmorillonite. In a common water treatment process for arsenic removal, As(III), if necessary, is readily oxidized into As(V) by conventional means (e.g., using O_2 and/or ozone, chlorine, and hydrogen peroxide, etc.) [14–16]. Hence, this research only focused on As(V) removal by Al_{13}-modified montmorillonites.

2. Materials and methods

2.1. Synthesis of hydroxyl Al modifiers

Hydroxyl Al modifiers with various basicities (i.e., 0, 2.0, and 2.2) were prepared by the micro-titrating method [17]. The resulting samples were denoted as AC, PAC_{20}, and PAC_{22}, respectively. Purified Keggin-Al_{13} modifier (PAl_{13}) was obtained from PAC_{22} by chemical purification [18]. The speciation of the hydroxyl Al modifiers was studied by ^{27}Al nuclear magnetic resonance (NMR) spectroscopy, and the detailed analysis procedure can be found in [17]. The concentration of total Al (Al_T) in each sample was detected by inductively coupled plasma-atomic emission spectroscopy (ICP-AES; PerkinElmer, USA).

2.2. Modification of montmorillonites

Montmorillonite was purchased from Fenghong Clay Chemicals Co., Ltd. (Zhejiang, China). Prior to use, the montmorillonite was converted into a Na-exchanged form (Na-Mont) by a previously described method [5]. The Al_{13}-modified montmorillonite was prepared as follows. A 500 mL aqueous slurry of Na-Mont (1 wt%) was prepared, and its pH was adjusted to 4.0 using 1.0 mol/L HNO_3. About 100 mL of Al_{13} (0.1 M) stock solution was slowly pumped under vigorous stirring into the Na-Mont aqueous slurry at a flow rate of 0.33 mL/min. The mixture was stirred for 24 h, and the solution pH was maintained at 4.0. After depositing for 12 h, the montmorillonite solids were separated by centrifugation at 5000 rpm for 30 min, washed several times with distilled water to remove excess electrolytes, dried at 60 °C, ground in an agate mortar, and passed through a 200-mesh sieve. The product was named Al_{13}-Mont. The AC- and PAC_{20}-modified montmorillonites were prepared in similar procedure, and the products were designated as AC-Mont and PAC_{20}-Mont, respectively.

2.3. Characterization of modified montmorillonites

The X-ray diffraction (XRD) patterns of the powered samples were obtained using a PANalytical X'Pert PRO MPD with Cu Kα radiation. The patterns were measured in the 2θ range of 4.5–80° at a step size of 0.033°. The surface area and pore size distribution were calculated from nitrogen adsorption–desorption isotherm data by the Brunauer–Emmett–Teller (BET) and Barret–Joyner–Halenda (BJH) methods using a Beishide 3H-2000P S2 apparatus. The isotherms were measured at 77 K using N_2. Before determining the isotherms, the samples were outgassed by heating at 423.15 K for 1 h under N_2 flow. An X-ray energy-dispersive spectrometer (S-4800, Hitachi) was used to analyze the chemical composition of the four montmorillonites. A Fourier-transform infrared spectrometry (FT-IR) system (Nicolet, Nexus 670) was used to determine the functional groups. The transmission spectrum was obtained at 64 scans with a 4 cm^{-1} resolution, and the spectrum was corrected with a KBr background.

2.4. Arsenate adsorption tests

Stock solutions of 1000 mg/L As(V) were prepared by dissolving the required amount of $Na_3AsO_4{\cdot}7H_2O$ in deionized doubly distilled water. The arsenate adsorption tests were carried out in triplicate using a batch method. About 0.05 g of the four absorbents were mixed with 25 mL of various As(V) concentrations (i.e., 5, 10, 20, 40, 70, 90, and 110 mg/L) in 100 mL-capacity sealed polypropylene centrifuge tubes. The mixture was shaken at 140 rpm at 25 °C for 12 h. The mixture pH was maintained at 6.9 by adding HNO_3 or NaOH. The products were centrifuged at 5000 rpm for 30 min, and filtered through a 0.45 μm cellulose acetate membrane. The filtrates were analyzed for residual As(V) concentrations by ICP-AES (PerkinElmer, USA).

2.5. As(V) adsorption kinetics

About 0.3 g of modified or unmodified montmorillonites was mixed with 10 mg/L As(V), and mechanical shaking was immediately performed. The pH of the mixture was maintained at 6.9 throughout the kinetics study. The As(V) concentrations of the mixture were determined 0, 5, 10, 20, 40, 60, 80, 120, 200, and 360 min after shaking.

3. Results and discussion

3.1. Physicochemical properties of the montmorillonites

The surface area, pore volumes, and average pore diameters of Na-Mont as well as the three other modified montmorillonites (i.e., AC-Mont, PAC_{20}-Mont, and Al_{13}-Mont) are listed in Table 1. The BET surface area of Na-Mont was initially 21.47 m^2/g, but it increased to 22.51, 169.1, and 267.7 m^2/g after modification with AC, PAC_{20}, and PAl_{13}, respectively. As inferred from the speciation of the hydroxyl-Al solutions by ^{27}Al NMR spectroscopy (Table 2), almost all Al species in AC were monomers (Al_m), whereas over 96% of PAl_{13} was Al_{13} species with Keggin structure. Therefore, it can be concluded from the two tables that the BET surface areas of the modified montmorillonites obviously increased with increased Al_{13} content in the modifiers. The BET surface areas increased more than 10 times after modification with the purified Al_{13} solution. There were minimal differences between the BET surface areas of Na- and AC-Mont, although AC-Mont was also modified with a hydroxyl Al solution. This phenomenon may further indicate that the Al_{13} species, not the monomers, in the hydroxyl Al solutions mainly contributed to the significant improvement of the surface areas of the modified montmorillonites.

Apart from the BET surface area, the micropore surface area, total pore volume, and micropore volume of Na-Mont and the three other modified montmorillonites also had similar distribution trends. Notably, the micropore surface area and volume of Na- and AC-Mont were not determined. Micropores are known to contribute to most of the adsorption capacity [19,20]. Hence, the

Table 1
Basal spacing (d_{001}), surface area, pore volume, and average pore diameter of Na-Mont, AC-Mont, PAC_{20}-Mont, and Al_{13}-Mont.

Adsorbent	d_{001} (Å)	BET surface area (m^2/g)	Micropore surface area (m^2/g)	Total pore volume (mL/g)	Micropore volume (mL/g)	Average pore diameter (nm)
Na-Mont	9.770	21.47	0.000	0.0865	0.000	10.95
AC-Mont	13.49	22.51	0.000	0.1060	0.000	8.640
PAC_{20}-Mont	18.59	169.1	76.29	0.2134	0.0477	7.040
Al_{13}-Mont	18.72	267.7	153.2	0.2041	0.1047	3.970

Table 2
Speciation of hydroxyl-Al solutions in ^{27}Al NMR spectroscopy.

Hydroxyl Al solutions	pH	^{27}Al NMR spectroscopy			ICP-AES
		Al_m (%)	Al_{13} (%)	Al_{un} (%)	Al_T (M)
AC	3.04	100	–	–	0.102
PAC_{20}	4.16	12.40	77.85	9.75	0.103
PAl_{13}	4.35	3.15	96.15	0.70	0.103

negligible micropore surface area and volume of Na- and AC-Mont may greatly decrease the adsorption capacity of the two adsorbents. After PAC_{20} and PAl_{13} were introduced into the interlayers of the montmorillonites, the micropore surface areas increased to 76.29 and 153.2 m^2/g, and the micropore volumes rose to 0.0477 and 0.1047 mL/g, respectively. These results could be ascribed to the introduction of Keggin-Al_{13} into the montmorillonites.

Compared with monomers, Al_{13} species have higher polymerization degrees and Keggin structures. When the two Al species were introduced into the montmorillonites, the Al_{13} species obtained larger interlayer distances, which accounted for the more significant improvement of the surface areas and pore volumes of the modified montmorillonites. This phenomenon was also confirmed by the XRD analysis results of the four adsorbents (Fig. 1). The basal spacings (d_{001}) of the four montmorillonites obtained from Fig. 1 are also listed in Table 1. Fig. 1 and Table 1 showed that the basal spacing of Na-Mont was 9.77 Å. For AC- and PAC_{20}-Mont, the *d* spacing increased to 13.49 and 18.59 Å, respectively. This finding indicated the replacement of native ions with comparatively larger and more hydrated Al particles (e.g., Al_{13}) in the interlayer. A previous research has calculated the spacing of Na-Mont at room temperature to be 9.90 Å [21], which is slightly higher than the 9.77 Å in the present study. Considering that all samples were dried at 60 °C, the decreased basal spacing to 9.77 Å may be attributed to the loss of water molecules from the interlayer spacing of Na-Mont [22]. The main chemical compositions of Na-Mont and the three modified montmorillonites were also studied by X-ray energy-dispersive spectrometry. After modification with the AC, PAC_{20}, and PAl_{13} solutions, the relative contents of Al in the modified montmorillonites increased to 10.93 wt%, 11.80 wt%, and 15.24 wt%, respectively, compared with 6.76 wt% of Na-Mont. On the other hand, the contents of exchangeable cations (e.g., Na and Ca) in the original montmorillonite decreased, indicating that these native cations were replaced by polyaluminum. A maximum basal spacing of 18.72 Å was observed in Al_{13}-Mont. This result also proved that a higher Al_{13} content was intercalated into the modified montmorillonite. The special molecular structure of Al_{13} may have caused the significantly increased basal spacing of Al_{13}-Mont. This special structure may also explain the decreased average pore diameters of the modified montmorillonites with increased Al_{13} content in the pillared reagents, which was not similar with the changes in the surface areas and pore volumes. The intercalation with higher Al_{13} content may have narrowed the lateral distance between the Al_{13} pillars, and consequently decreased the pore diameter [4,5].

Changes in the physicochemical properties of the modified montmorillonites were also inferred from the FT-IR spectra in Fig. 2. The FT-IR spectra of the four montmorillonites showed a broad absorption band near 3420 cm^{-1} in every spectrum, which was assigned to the H—O—H stretching vibration [23]. After the intercalation of PAC_{20} and PAl_{13} into the montmorillonites, the

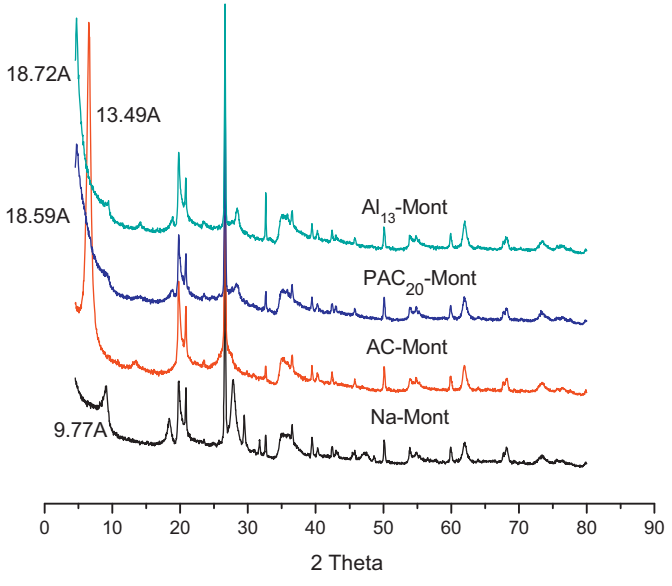

Fig. 1. Powder XRD patterns of Na-Mont, AC-Mont, PAC_{20}-Mont, and Al_{13}-Mont after drying at 60 °C for 24 h.

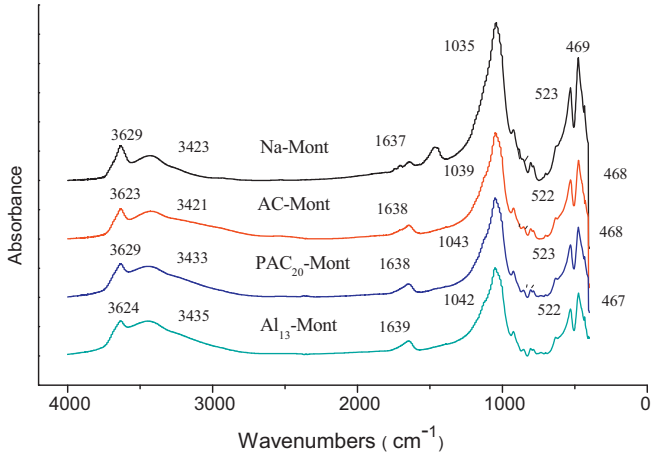

Fig. 2. FT-IR spectra of Na-Mont, AC-Mont, PAC_{20}-Mont, and Al_{13}-Mont.

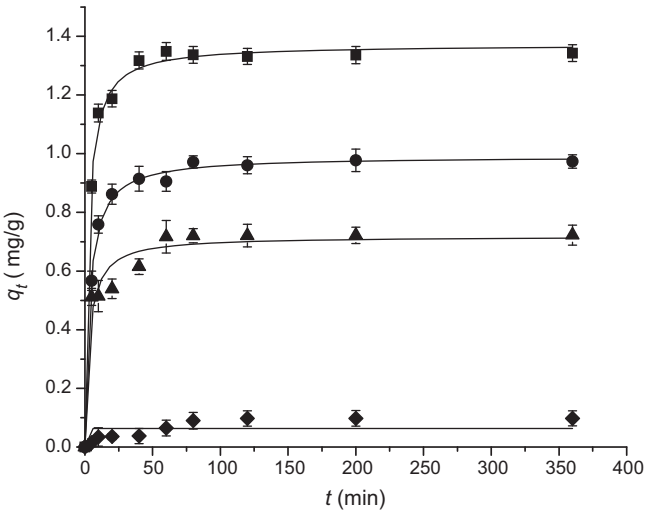

Fig. 3. Pseudo-second-order sorption kinetics of arsenate adsorbed onto Na-Mont (♦), AC-Mont (▲), PAC_{20}-Mont (●), and Al_{13}-Mont (■).

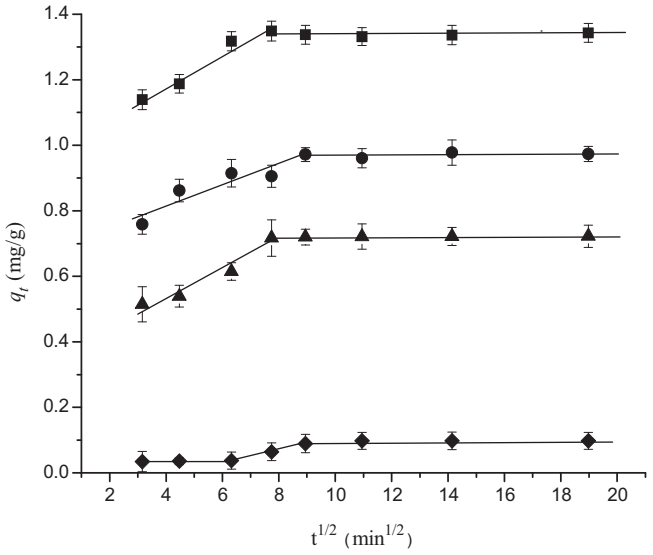

Fig. 4. Intraparticle diffusion model fits of arsenate adsorbed onto Na-Mont (♦), AC-Mont (▲), PAC_{20}-Mont (●), and Al_{13}-Mont (■).

band at 3423 cm^{-1} shifted to 3433 and 3435 cm^{-1}, respectively. These significant shifts were mainly ascribed to the Al_{13} species in the two modified montmorillonites. With the shifts from 1035 to 1042 cm^{-1} near the complex Si—O stretching vibration in the tetrahedral sheet, the intensity also decreased from Na- to Al_{13}-Mont. This finding confirmed that Al_{13} species were intercalated into the interlayers of the montmorillonites, which well agreed with the results obtained by O—H vibration analyses.

3.2. Adsorption kinetics of As(V) on unmodified and modified montmorillonites

The adsorption kinetics of As(V) in the four montmorillonite adsorbents are shown in Fig. 3. Adsorption kinetics is one of the most important characteristics that define adsorption efficiency, and describes the rates (slopes of the plot) of As(V) retention. The modified montmorillonites showed enhanced rates of As(V) adsorption compared with Na-Mont, and Al_{13}-Mont possessed the highest adsorption rate. The majority of As(V) particles was removed within the first 20 min of contact with the adsorbents, After 40 min of contact with Al_{13}-Mont, the adsorption nearly ceased, indicating the attainment of equilibrium. For Na-Mont, equilibrium attainment took 80 min. The amounts of As(V) adsorbed onto the four adsorbents followed the trend Al_{13}-Mont > PAC_{20}-Mont > AC-Mont > Na-Mont, which well agreed with the distribution characteristics of Al_{13} content in the modified reagents and modified montmorillonites (Table 2).

To further evaluate the kinetic mechanism of the adsorption process, the pseudo-first-order [24,25], pseudo-second-order [26], and intraparticle diffusion models [27] were used to interpret the experimental phenomena, as respectively shown in the following equations:

$$\frac{1}{q_t} = \frac{1}{q_1} + \frac{k_1}{q_1 t}, \tag{1}$$

$$\frac{t}{q_t} = \frac{1}{k_2 q_2^2} + \frac{1}{q_2} t, \tag{2}$$

$$q_t = k_p t^{1/2} + C, \tag{3}$$

where k_i (i = 1, 2, and p) represents the corresponding kinetics rate constants (min^{-1}, g/mg min, and mg/g $min^{1/2}$), q_i (i = 1, 2, and t) represents the amount of As(V) adsorbed (mg/g) at equilibrium and time t (min), and C is the intercept of the intraparticle diffusion model.

The kinetic parameters for the adsorption of As(V) onto the four adsorbents are given in Table 3. The experimental results on the As(V) amounts adsorbed at equilibrium conformed with those calculated by the abovementioned models. The kinetic data better fitted the pseudo-second-order model ($R_2^2 > 0.95$), suggesting that the adsorption process may be chemisorption [28–30]. From Table 3, both the rate constant and As(V) amounts adsorbed at equilibrium were also inferred to decrease with decreased Al_{13} content in the modified montmorillonites. Therefore, the intercalation of Al_{13} into montmorillonites improved not only the adsorption rate, but also the adsorption capacity of the adsorbents.

Table 3 shows that the Na-Mont adsorption data better fitted the intraparticle diffusion model than the three other modified montmorillonites. The adsorption process can be divided into three steps, namely, external surface diffusion, intraparticle diffusion, and final equilibrium. Fig. 4 shows that there were indeed three steps for Na-Mont; the rate-limiting processes appeared to be external surface and intraparticle diffusions. In comparison, the adsorption processes of the modified montmorillonites involved only two stages, indicating that external surface diffusion may be a rapid process considering the relatively slow process of intraparticle diffusion. The diffusion rate of Al_{13}-Mont for As(V) was faster than that of Na-Mont, suggesting that the As(V) ions were more easily diffused and transported in the pores of Al_{13}-Mont than in those of Na-Mont [5,31].

3.3. Adsorption mechanism of As(V) on unmodified and modified montmorillonites

3.3.1. Adsorption isotherms

The As(V) adsorption isotherms of the four montmorillonites are presented in Fig. 5. Different adsorption isotherms (Langmuir [32], Freudlich [33], and Redlich–Peterson [34]) were used to analyze the adsorption data to explain the differences among the adsorption mechanisms of the four montmorillonites. The Langmuir, Freudlich, and Redlich–Peterson isotherm equations are shown in the following equations, respectively:

$$q_e = \frac{bq_m C_e}{1 + bC_e}, \tag{4}$$

Table 3
Pseudo-first-order, pseudo-second-order, and intraparticle diffusion kinetic parameters for the adsorption of arsenate on Na-Mont, AC-Mont, PAC_{20}-Mont, and Al_{13}-Mont.

Model	Parameter	Al_{13}-Mont	PAC_{20}-Mont	AC-Mont	Na-Mont
Pseudo-first-model	k_1 (min^{-1})	0.2099	0.1699	0.2021	0.0197
	q_1 (mg/g)	1.318	0.9434	0.6794	0.1009
	R_1^2	0.9899	0.9895	0.9084	0.9362
Pseudo-second-model	k_2 (mg/g min)	1.327	0.9837	0.2481	0.0269
	q_2 (mg/g)	3.516	3.538	1.966	1.415
	$R_2{}^2$	0.9516	0.9633	0.9665	0.9517
Intraparticle diffusion model	k_p (mg/g $min^{-1/2}$)	0.0468	0.0366	0.0276	0.0058
	C (mg/g)	0.7622	0.5069	0.3653	0.0122
	R_p^2	0.4175	0.4847	0.5186	0.8224

$$q_e = K_f C_e^{1/n}, \tag{5}$$

$$q_e = \frac{AC_e}{1 + BC_e{}^g}, \tag{6}$$

C_e is the equilibrium concentration of As(V) (mg/L); q_e and q_m are the equilibrium and maximum amounts of As (V) adsorbed (mg/g), respectively; b is the sorption equilibrium constant (L/mg); K_f and n are constants reflecting the adsorption capacity and adsorption intensity, respectively; A, B, and g are isotherm constants.

The fitted parameters and regression coefficients of the three models are presented in Table 4. All models fairly well fitted the adsorption data, with the Freundlich and Redlich–Peterson isotherms showing better fits. The Redlich–Peterson isotherm is known as essentially a Freundlich isotherm [35], and the R^2 values acquired for both isotherms were above 0.95, indicating good mathematical fits. Trebal [36] has proposed that adsorption benefits when the n value of the Freundlich isotherm falls within 1–10. In the present experiment, the n values were 3.5162, 3.5388, 1.9666, and 1.4155 for Al_{13}-, PAC_{20}-, AC-, and Na-Mont, respectively. These results indicated that these adsorptions were favorable. The g values of the Redlich–Peterson isotherms tended to approach 1 (>0.7187), signifying that the isotherms were approaching the Langmuir form. However, g of Na-Mont was 0.3827, indicating that the isotherm was approaching Henry's law.

Table 4 shows that the adsorption capacity for As(V) of Al_{13}-Mont was the best, and that of Na-Mont was the poorest. This result was consistent with those of the BET surface area and adsorption kinetics analyses. The highly enhanced capacity of Al_{13}-Mont may be attributed to its larger micropore surface area, micropore volume, and basal spacing (d_{001}). The high positive charge of Al_{13} species also contributed to the high adsorption capacity of Al_{13}-Mont. As(V) often exists as an anion in solutions [37]. As for Na-Mont, the native ion is Na^+ and only one positive charge is carried by the ion. However, the intercalated monomeric Al and Al_{13} with their +3 and +7 charges [38,39] certainly had higher electrostatic attractions for As(V).

3.3.2. Energy of sorption

The mean sorption energy E (kJ/mol) can often provide information on chemical and physical sorption. E can be calculated by the Dubinin–Radushkevich (D–R) adsorption isotherm parameters. The linear form of the D–R isotherm equation is:

$$\ln\ q_e = \ln\ q_t - \beta\varepsilon^2, \tag{7}$$

β is a constant related to the mean free energy of adsorption per mole of the adsorbate ($mol^2\ J^{-2}$); q_e and q_t are the equilibrium and theoretical saturation capacities (mol g), respectively; ε is the Polanyi potential, which is equal to $RT\ln[1 + (1/C_e)]$. Where R ($J\ mol^{-1}\ K^{-1}$) is the gas constant and T (K) is the absolute temperature. Hence, by plotting $\ln q_e$ against ε^2, q_t ($mol\ g^{-1}$) can be obtained from the intercept, and β can be obtained from the slope. The free energy E (kJ/mol) can then be calculated from the relationship:

$$E = \frac{1}{(2\beta)^{1/2}}. \tag{8}$$

The adsorption process follows chemical sorption when E ranges from 8 kJ/mol to 16 kJ/mol. When $E < 8$ kJ/mol, the adsorption process becomes physical. As calculated from Fig. 6, the E values of AC-, PAC_{20}-, and Al_{13}-Mont were 9.128, 12.90, and 15.81 kJ/mol, respectively, implying chemical adsorption mechanisms. However, E of Na-Mont was 7.071 kJ/mol, implying physical sorption. These

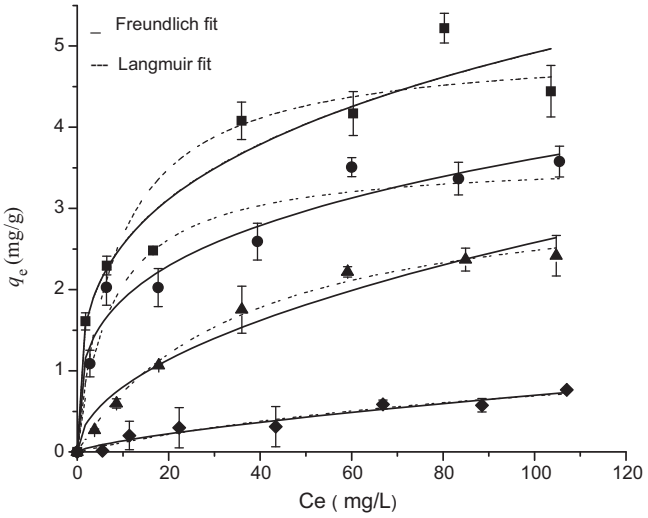

Fig. 5. Freundlich and Langmuir adsorption isotherms of arsenate adsorbed onto Na-Mont (♦), AC-Mont (▲), PAC_{20}-Mont (●), and Al_{13}-Mont (■).

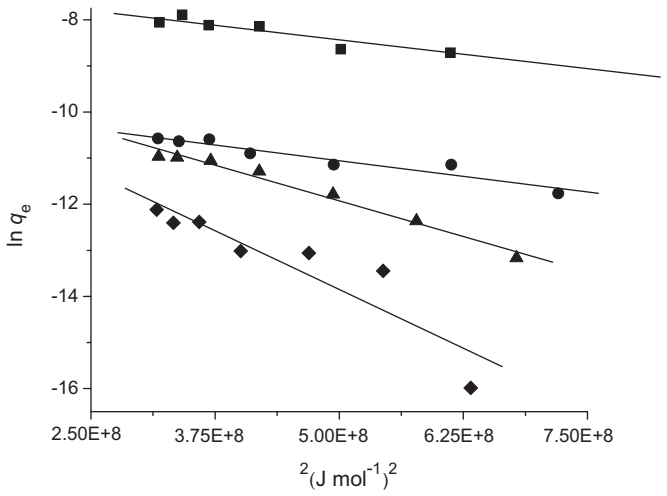

Fig. 6. Dubinin–Radushkevich (D–R) plots for the adsorption of arsenate onto Na-Mont (♦), AC-Mont (▲), PAC_{20}-Mont (●), and Al_{13}-Mont (■).

Table 4
Langmuir, Freudlich and Redlich–Peterson constants and correlation coefficients for the adsorption of arsenate on Na-Mont, AC-Mont, PAC_{20}-Mont, and Al_{13}-Mont.

Model	Parameter	Al_{13}-Mont	PAC_{20}-Mont	AC-Mont	Na-Mont
Langmuir model	q_m (mg/g)	5.008	3.610	3.370	1.532
	b (L/mg)	0.1147	0.1321	0.0279	0.0081
	R_1^2	0.9154	0.9341	0.9947	0.9468
Freundlich model	K_f	1.327	0.9837	0.2481	0.0269
	n	3.516	3.538	1.966	1.415
	R_f^2	0.9516	0.9633	0.9665	0.9517
Redlich–Peterson model	A	43.30	2.557	0.0704	0.0404
	B	32.13	2.164	0.0024	0.8268
	g	0.7187	0.7560	1.449	0.3827
	R_r^2	0.9515	0.9643	0.9997	0.9519
Dubinin–Radushkevich model	β (mol^2 kJ^{-2})	2.00×10^{-3}	3.01×10^{-3}	6.00×10^{-3}	10.01×10^{-3}
	E (KJ mol^{-1})	15.81	12.90	9.128	7.071
	R_{D-R}^2	0.9306	0.9185	0.9794	0.8363

discrepancies in sorption mechanisms can be ascribed to the introduction of Al_{13} or monomeric Al into the montmorillonites. The mean sorption energy of Al_{13}-Mont was also higher than that of Na-Mont, implying that Al_{13}-Mont had a higher affinity for As(V), corresponding to the results of the adsorption kinetics and isotherms. This can also be explained by the structure characteristics of Al_{13}. Generally, Al_{13} has large amount of hydroxyls in the outer trimmers (i.e., μ_2-OH, μ_2-OH and η-OH). The hydroxyls between Al_{13} and arsenate could bridge together and electron also transferred from arsenate to Al_{13} molecular. The whole process was observed to be chemical adsorption. Perhaps, the changes in the adsorption mechanism of the four adsorbents were mainly ascribed to the difference in hydroxyl number in modifiers.

It can be seen from Table 3 and Table 4, the correlation coefficients (R^2) for the intraparticle diffusion model and Dubinin–Radushkevich model were a little lower. Similar phenomenon can also be found in some previous studies [40,41]. The main reasons were ascribed to the difference in physicochemical characteristics of the four absorbents and the shortages of the models [42]. Even so, the two models are still the best method to probe the adsorption process to date.

3.4. Contributions of the high purity and high positive charger of Keggin-Al_{13}

3.4.1. Uniform pore structure formed by high-purity Al_{13}

Pore size distribution is considered to be a good indicator of the uniformity of porous materials. In the present study, the pore size distribution and relative contribution of different pore size ranges to the BJH pore volume of the four adsorbents were compared. The purpose was to investigate the differences in pore uniformity.

As shown in Fig. 7, Na- and AC-Mont had relatively wide pore size distributions, ranging from 0 nm to 26.43 and 25.76 nm, respectively. With the introduction of Al_{13}, the pore size range of PAC_{20}-Mont decreased only in the 0 nm to 15.05 nm region. However, for Al_{13}-Mont, the pore size range was mainly restricted to

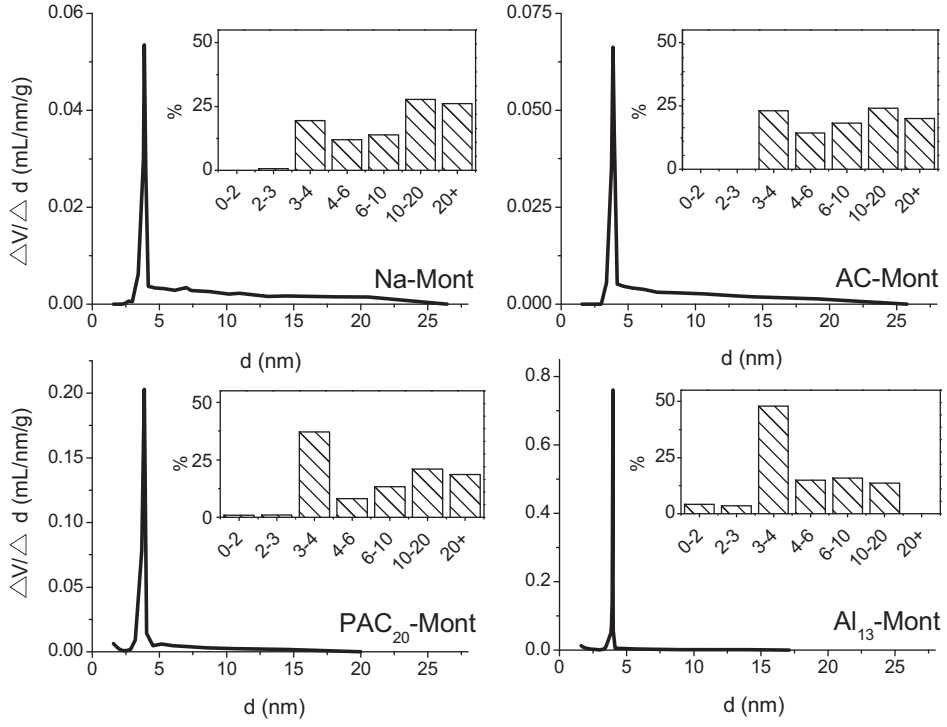

Fig. 7. Pore size distribution and relative contribution of different pore size ranges to the BJH pore volume (inset) of Na-Mont, AC-Mont, PAC_{20}-Mont, and Al_{13}-Mont.

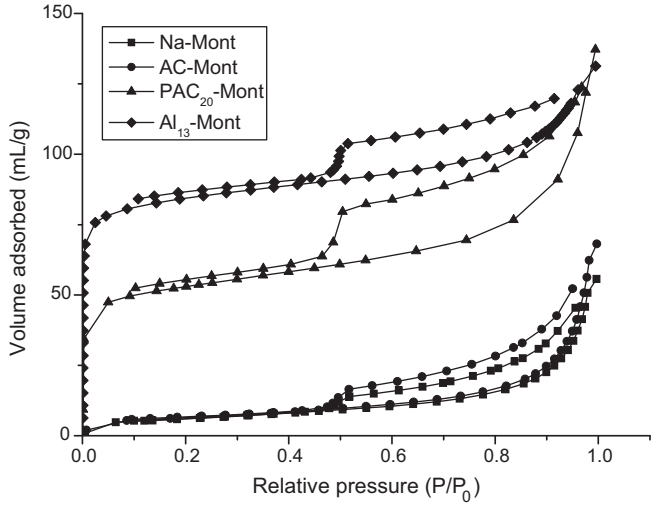

Fig. 8. Nitrogen adsorption–desorption isotherms for Na-Mont, AC-Mont, PAC_{20}-Mont, and Al_{13}-Mont.

narrower regions (i.e., 0 nm to 5.11 nm), which may indicate that Al_{13}-Mont had a more highly uniform pore structure. In fact, diverse pore sizes in montmorillonite adsorbents often result in the formation of numerous pores with bottleneck shapes, thereby retarding the As(V) trapping process. Therefore, the very high affinity of Al_{13}-Mont for As(V) can be explained by the uniformity of the pore structure.

Apart from pore size distribution, the relative volume fraction of pores with different size ranges can further elucidate the pore structure uniformity of Al_{13}-Mont. Generally, if a predominant fraction of pores with a certain narrow size range exists in a porous material, these pores may be the major contributors to the total pore volume. If a dominant number of pores have similar sizes in a porous material, the material can be thought of as uniform [43]. The insets in Fig. 7 illustrate the relative fractions to the BJH pore volumes of the pore sizes with different ranges (i.e. 0–2 nm, 2–3 nm, 3–4 nm, 4–6 nm, 6–10 nm, 10–20 nm, and over 20 nm) of the four montmorillonites. Comparatively uniform distributions of the contribution (%) were detected in Na- and AC-Mont. However, the uniform distribution only implied that distinct pore structures with close amounts existed in the interlayers of the montmorillonites. The highest pore uniformity was found in Al_{13}-Mont because 3 nm to 4 nm-sized pores contributed about 50% of the total pore volume. Pores with larger sizes are expected to possess higher pore volumes. In the present study, the highest contribution (%) of pore volume was mainly ascribed to the 3 nm to 4 nm pores. However, the pores with this size range may not have larger pore volumes compared with larger pores (e.g., 4 nm to 6 nm or larger). If this factor is taken into consideration, the uniformity of the pore structure of Al_{13}-Mont may be more outstanding. Therefore, the intercalation of high-purity Al_{13} greatly improved the uniformity of pore structure, and thereby could greatly enhance the diffusion and adsorption rates of As(V) [13].

The uniformity of Al_{13}-Mont can also be inferred from the nitrogen adsorption–desorption isotherms in Fig. 8. In the isotherms of PAC_{20}- and Al_{13}-Mont, sharp inflections of adsorbed volumes at about 0.5 relative pressures (P/P_0) were detected. The sharpness of these steps also implied that the mesopores of the samples were uniform. Conversely, Na- and AC-Mont exhibited poor uniformity given that shoulders were observed in the desorption branch of the hysteresis loop [13].

3.4.2. Role of Keggin-Al_{13} in As(V) adsorption

To describe more clearly the role of Keggin-Al_{13} in the As(V) adsorption performance of the montmorillonites, the micropore surfaces, micropore volumes, BET surface areas, and adsorption capacities of the montmorillonites modified with hydroxyl Al solutions of different Al_{13} content were further compared (Fig. 9).

Fig. 9 reveals that with increased intercalated Al_{13} content, the structure and adsorption capacity of the montmorillonites for As (V) significantly improved. Although Na- and AC-Mont have similar BET surface areas, micropore surface areas, and micropore

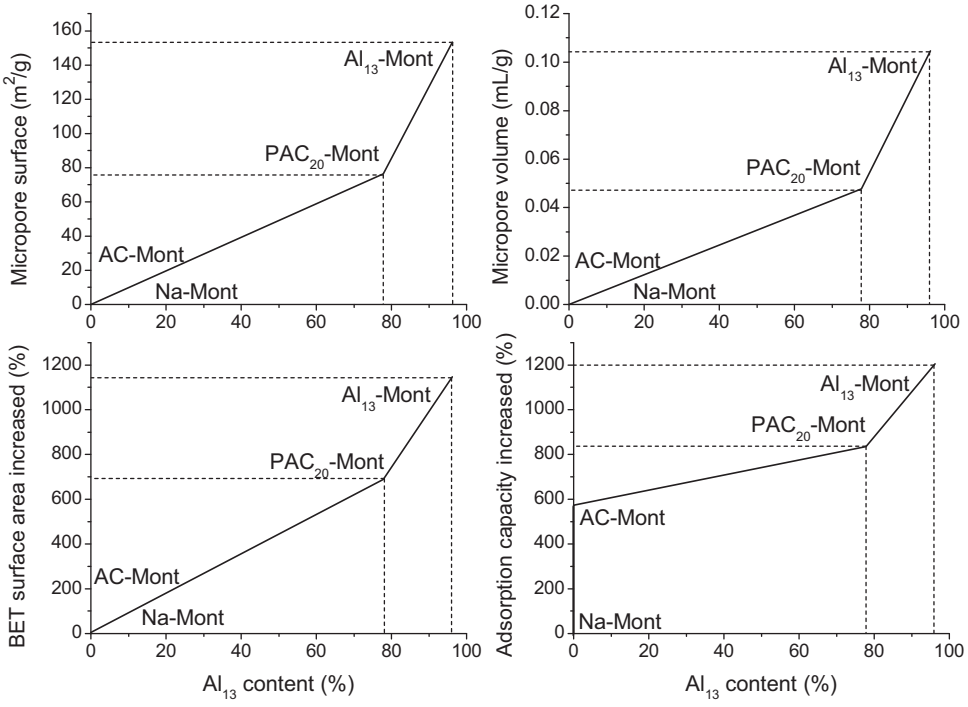

Fig. 9. Variations of micropore surface, micropore volume, BET surface area and adsorption capacity for arsenate of montmorillonites modified with different content of Al_{13}.

volumes, the adsorption capacity of AC-Mont was about 573% higher than that of Na-Mont. The higher positive charge carried by the monomeric Al species may have greatly improved the electrostatic attraction of the modified montmorillonite for As(V). PAC_{20}- and Al_{13}-Mont had even higher affinities (835% and 1206%, respectively) for As(V) than Na-Mont. These obvious increases can be mainly attributed to the introduction of Al_{13} into the montmorillonites. Al_{13} had a higher positive charge (+7) than monomeric Al (+3) and Na (+1) Hence, the experimental results further proved the role of the high positive charge of Al_{13} in the enhancement of adsorption performance of the modified montmorillonites.

Moreover, the micropore surface area and micropore volume of PAC_{20}-Mont also increased from 0 of Na- and AC-Mont to 76.29 m^2/g and 0.0477 mL/g, respectively, which could may also be attributed to the 77.85% intercalated Al_{13}. When the content of Al_{13} increased to 96.15% in PAl_{13}, the micropore surface area and micropore volume of Al_{13}-Mont further dramatically increased to 153.2 m^2/g and 0.1047 mL/g, respectively. This result is obviously caused by the additional 18.3% Al_{13} in the modifier. The 18.3% increase in Al_{13} purity also played a disproportionate role in enhancing the performance of the modified montmorillonites. The additional 18.3% Al_{13} content in Al_{13}-Mont resulted in an even higher contribution than the 77.85% Al_{13} content in PAC_{20}-Mont. Fig. 9 also reveals significant and intense improvements in physicochemical properties and adsorption performances with increased Al_{13} in the modified montmorillonites. These findings may prove that besides the high positive charge of Al_{13}, its high purity also plays an important role in the modification of montmorillonites.

4. Conclusions

Al_{13}-modified montmorillonites are highly active in arsenate removal. The high positive charge, high purity, and special Keggin structure of Keggin-Al_{13} enabled it to play a significant role in improving the physicochemical properties and As(V) adsorption performance of modified montmorillonites. The superiority of the structural properties and adsorption performances of the four adsorbents followed the trend Al_{13}-Mont > PAC_{20}-Mont > AC-Mont > Na-Mont. The adsorption mechanism of the modified montmorillonites for arsenate removal changed from physical to chemical due to the intercalation of mono Al or Al_{13}.

Acknowledgments

This research was supported by the National Basic Research Program of China (973 Project, 2010CB429003), NSFC (21007004), Major Science and Technology Program for Water Pollution Control and Treatment (2008ZX07209-007), and the Fundamental Research Funds for the Central Universities.

References

[1] World Health Organization, Guidelines for Drinking-Water Quality, World Health Organization, Switzerland, 2004.
[2] M. Jang, S.H. Min, T.H. Kim, J.K. Park, Removal of arsenite and arsenate using hydrous ferric oxide incorporated into naturally occurring porous diatomite, Environ. Sci. Technol. 40 (2006) 1636–1643.
[3] M. Kanematsu, T.M. Young, K. Fukushi, P.G. Green, J.L. Darby, Extended triple layer modeling of arsenate and phosphate adsorption on a goethite–based granular porous adsorbent, Environ. Sci. Technol. 44 (2010) 3388–3394.
[4] A. Ramesh, H. Hasegawaa, T. Makia, K. Uedaa, Adsorption of inorganic and organic arsenic from aqueous solutions by polymeric Al/Fe modified montmorillonite, Sep. Purif. Technol. 56 (2007) 90–100.
[5] L.G. Yan, X.Q. Shan, B. Wen, G. Owens, Adsorption of cadmium onto Al_{13}-pillared acid-activated montmorillonite, J. Hazard. Mater. 156 (2008) 499–508.
[6] P. Na, X.M. Jia, B. Yuan, Y. Li, J.Y. Na, Y.C. Chen, L.S. Wang, Arsenic adsorption on Ti-pillared montmorillonite, J. Chem. Technol. Biotechnol. 85 (2010) 708–714.
[7] C. Luengoa, V. Pucciaa, M. Avena, Arsenate adsorption and desorption kinetics on a Fe (III)-modified montmorillonite, J. Hazard. Mater. 186 (2011) 1713–1719.
[8] H.F. Liu, D.R. Miao, F. Liu, Preparation of an iron oxide modified montmorillonite for removal of arsenic in waters, Adv. Mater. Res. 156 (2011) 849–853.
[9] R.M. Dhobleb, S. Lungea, A.G. Bholec, S. Rayalu, Magnetic binary oxide particles (MBOP): a promising adsorbent for removal of As(III) in water, Water Res. 45 (2011) 4769–4781.
[10] Z.H. Li, J.S. Jean, W.T. Jiang, P.H. Chang, C.J. Chen, L.B. Liao, Removal of arsenic from water using Fe-exchanged natural zeolite, J. Hazard. Mater. 187 (2011) 318–323.
[11] R.L. Zhu, T. Wang, F. Ge, W.X. Chen, Z.M. You, Intercalation of both CTMAB and Al_{13} into montmorillonite, J. Colloid Interface Sci. 335 (2009) 77–83.
[12] Z.H. Qin, P. Yuan, J.X. Zhu, H.P. He, D. Liu, S.Q. Yang, Influences of thermal pretreatment temperature and solvent on the organosilane modification of Al_{13}-intercalated/Al-pillared montmorillonite, Appl. Clay Sci. 50 (2010) 546–553.
[13] E.W. Shin, J.S. Han, Phosphate adsorption on aluminum-impregnated mesoporous silicates: surface and behavior of adsorbents, Environ. Sci. Technol. 38 (2004) 912–917.
[14] M.J. Scott, J.J. Morgan, Reactions at oxide surfaces. 1. Oxidation of As (III) by synthetic birnessite, Environ. Sci. Technol. 29 (1995) 1898–1905.
[15] M. Bissen, M. Vieillard-Baron, A.J. Schindelin, F.H. Frimmel, TiO_2-catalyzed photooxidation of arsenite to arsenate in aqueous samples, Chemosphere 44 (2001) 751–757.
[16] L.F. Yin, J.F. Niu, Z.Y. Shen, J. Chen, Mechanism of reductive decomposition of pentachlorophenol by Ti-doped β-Bi_2O_3 under visible light irradiation, Environ. Sci. Technol. 44 (2010) 5581–5586.
[17] C.H. Feng, H.X. Tang, D.S. Wang, Differentiation of hydroxyl-aluminum species at lower OH/Al ratios by combination of ^{27}Al NMR and Ferron assay improved with kinetic resolution, Colloids Surf. A 305 (2007) 76–82.
[18] Y. Xu, D.S. Wang, H. Liu, Y.Q. Lu, H.X. Tang, Optimization of the separation and purification of Al_{13}, Colloids Surf. A 231 (2003) 1–9.
[19] M.G. Nijkamp, J.E.M.J. Raaymakers, A.J. van Dillen, K.P. de Jong, Hydrogen storage using physisorption–materials demands, Appl. Phys. A 72 (2001) 619–623.
[20] H.L. Wang, Q.M. Gao, J. Hu, High hydrogen storage capacity of porous carbons prepared by using activated carbon, J. Am. Chem. Soc. 131 (2009) 7016–7022.
[21] D.L. Ho, R.M. Briber, C.J. Glinka, Characterization of organically modified clays using scattering and microscopy techniques, Chem. Mater. 13 (2001) 1923–1931.
[22] O.S. Ahmeda, D.K. Dutta, In situ generation of metal clusters in interlamellar spacing of montmorillonite clay and their thermal behaviour, Thermochim. Acta. 395 (2003) 209–216.
[23] V.M. Malhotra, A.A. Ogloza, FTIR spectra of hydroxyls and dehydroxylation kinetics mechanism in montmorillonite, Phys. Chem. Miner. 16 (1989) 386–393.
[24] Y.S. Ho, G. McKay, Sorption of dye from aqueous solution by peat, Chem. Eng. J. 70 (1998) 115–124.
[25] Y.S. Ho, G. McKay, The kinetics of sorption of basic dyes from aqueous solution by sphagnum moss peat, Can. J. Chem. Eng. 76 (1998) 822–827.
[26] Y.S. Ho, G. McKay, Kinetic models for the sorption of dye from aqueous solution by wood, Process Saf. Environ. Protect 76 (1998) 183–191.
[27] W.J Weber, J.C. Morris, Kinetics of adsorption on carbon from solution, J. Sanit. Eng. Div. Am. Soc. Civ. Eng. 89 (1963) 31–60.
[28] X.J. Guo, F.H. Chen, Removal of arsenic by bead cellulose loaded with iron oxyhydroxide from groundwater, Environ. Sci. Technol. 39 (2005) 6808–6818.
[29] J.M. Jang, E.W. Shin, J.K. Park, S. Choi, Mechanisms of arsenate adsorption by highly-ordered nano-structured silicate media impregnated with metal oxides, Environ. Sci. Technol. 37 (2003) 5062–5070.
[30] Q. Li, N.J. Easter, J.K. Shang, As(III) removal by palladium-modified nitrogen-doped titanium oxide nanoparticle photocatalyst, Environ. Sci. Technol. 43 (2009) 1534–1539.
[31] Y. Kim, C. Kim, I. Choi, S. Rengaraj, J. Yi, Arsenic removal using mesoporous alumina prepared via a templating method, Environ. Sci. Technol. 38 (2004) 924–931.
[32] I. Langmuir, The constitution and fundamental properties of solids and liquids, J. Am. Chem. Soc. 38 (1916) 2221–2295.
[33] H. Freundlich, Over the adsorption in solution, J. Phys. Chem. 57 (1906) 385–470.
[34] O. Redlich, D.L. Peterson, A useful adsorption isotherm, J. Phys. Chem. 63 (1959) 1024.
[35] D.G. Kinniburgh, General purpose adsorption isotherms, Environ. Sci. Technol. 20 (1986) 895–904.
[36] R.E. Trebal, Mass Transfer Operations, McGrew Hill, New York, USA, 1980.
[37] D. Mohan, C.U. Pittman, Arsenic removal from water/wastewater using adsorbents – a critical review, J. Hazard. Mater. 142 (2007) 1–53.
[38] M.Q. Yan, D.S. Wang, J.H. Qu, J.R. Ni, C.W.K. Chow, Enhanced coagulation for high alkalinity and micro-polluted water: the third way through coagulant optimization, Water Res. 42 (2008) 2278–2286.
[39] J.L. Lin, C.P. Huang, C.J.M. Chin, J.R. Pan, The origin of Al(OH)3-rich and Al13-aggregate flocs composition in PACl coagulation, Water Res. 43 (2009) 4285–4295.

[40] S.V. Mohan, S.V. Ramanaiah, B. Rajkumar, P.N. Sarma, Biosorption of fluoride from aqueous phase onto algal *Spirogyra* IO1 and evaluation of adsorption kinetics, Bioresour. Technol. 98 (2007) 1006–1011.
[41] M. Greluk, Z. Hubicki, Sorption of SPADNS azo dye on polystyrene anion exchangers: Equilibrium and kinetic studies, J. Hazardous Mater. 172 (2009) 289–297.
[42] N. Priyantha, A. Bandaranayaka, Investigation of kinetics of Cr(VI)-fired brick clay interaction, J. Hazardous Mater. 188 (2011) 193–197.
[43] N.G. Shang, F.C.K. Au, X.M. Meng, C.S. Lee, I. Bello, S.T. Lee, Uniform carbon nanoflake films and their field emissions, Chem. Phys. Lett. 358 (2002) 187–191.